Marine Geology 405 (2018) 1–11

Contents lists available at ScienceDirect

Marine Geology

journal homepage: www.elsevier.com/locate/margo

Analysing decadal-scale crescentic bar dynamics using satellite imagery: A case study at Anmok beach, South Korea

Panagiotis Athanasiou[a,*], Wiebe de Boer[a,b], Jeseon Yoo[c], Roshanka Ranasinghe[d,a,e], Ad Reniers[b]

[a] Deltares, P.O. Box 177, 2600, MH, Delft, The Netherlands
[b] Civil Engineering and Geosciences, Delft University of Technology, P.O. Box 5048, 2600, GA, Delft, The Netherlands
[c] Korean Institute of Ocean Science and Technology (KIOST), P.O. Box 426-744, Republic of Korea
[d] IHE Delft Institute for Water Education, P.O. Box 3015, 2601, DA, Delft, The Netherlands
[e] Water Engineering and Management, Faculty of Engineering Technology, University of Twente, PO Box 217, 7500, AE, Enschede, The Netherlands

ARTICLE INFO

Editor: E Anthony

Keywords:
Crescentic sandbars
Satellite imagery
Sandbar dynamics
Human interventions
Anmok beach

ABSTRACT

Understanding long-term sandbar dynamics can be crucial for informed coastal zone management, but is often hampered by data availability. To increase the number of sandbar observations available from bathymetric surveys, this study proposes and evaluates a method to manually extract the sandbar location using freely available satellite imagery for the case study of Anmok beach in South Korea. Validation of the satellite extracted sandbar locations against 9 in-situ measurements shows good agreement with errors well within the pixel resolution of the satellite imagery (i.e. 30 m for Landsat missions). The applicability of the method is constrained to locations where (1) the cross-shore crescentic length scales are larger than the image resolution, (2) frequent wave breaking and clouds are absent and (3) the water clarity is sufficient to enable the manual extraction of the sandbar crest line. Using the additional sandbar observations from the satellite imagery significantly increases the temporal extent and resolution of the dataset for Anmok beach. This allows the study of sandbar characteristics, dynamics and impacts of human interventions to an extent that would not have been possible without the satellite imagery. Within the study period 1990–2017 it is found that the sandbar maintains a persistent crescentic pattern that is only altered during prolonged and very intense storm conditions. The cumulative alongshore migration of the sandbars is investigated and found to be in the order of hundreds of meters over the 27 years study period. Comparing the sandbar characteristics prior and after the construction of Gangneung port shows that both the amplitudes and wavelengths of the sandbar crescents near the port have decreased after its construction.

1. Introduction

A variety of complex morphological patterns can emerge in the surf zone of sandy beaches, as a result of the spatial and temporal variability in hydrodynamics and sediment transport. One example of these patterns are crescentic sandbars, which show an alongshore rhythmic shape, characterized by alternating shoals and troughs, defined as sandbar horns and bays respectively (van Enckevort et al., 2004). In turn, these sandbar patterns affect the local hydrodynamics and, as a result, the beach morphodynamics. This morphological coupling between sandbar and beach (or shoreline) patterns has been previously highlighted (Sonu, 1973; Wright and Short, 1984; Coco et al., 2005; Orzech et al., 2011; Van de Lageweg et al., 2013). As the sandbars can affect the beach width, understanding sandbar dynamics is important for informed coastal zone management.

The inter- and intra-site variability of sandbar patterns length scales, both in the cross-shore and alongshore direction, have been previously given a lot of attention (Caballeria et al., 2002; van Enckevort et al., 2004; Ribas et al., 2007; Almar et al., 2010; Castelle et al., 2010). Furthermore, the alongshore migration of morphological features has been associated with the wave-driven alongshore current (Ruessink et al., 2000; Holman et al., 2006; Orzech et al., 2010). On the other hand, the effects of human interventions on nearshore sandbar patterns have seldom been studied so far (Bouvier et al., 2017; Rutten et al., 2018). The development of a technique that uses video imagery to extract the location of sandbars based on wave dissipation (Lippmann and Holman, 1989), gave rise to a large number of studies focusing on the sandbar patterns and its dynamics (Lippmann and Holman, 1990; van Enckevort et al., 2004; Plant et al., 2006; Pape et al., 2010; Splinter et al., 2011; Van de Lageweg et al., 2013; Price et al., 2014). Other

* Corresponding author at: Deltares, Boussinesqweg 1, 2629, HV, Delft, The Netherlands.
E-mail address: Panos.Athanasiou@deltares.nl (P. Athanasiou).

https://doi.org/10.1016/j.margeo.2018.07.013
Received 28 January 2018; Received in revised form 27 July 2018; Accepted 31 July 2018
Available online 04 August 2018
0025-3227/

studies used multiple bathymetric surveys through time to quantify the migration of sandbars (Plant et al., 1999; Ruessink et al., 2007b; Kuriyama et al., 2008; Walstra et al., 2012, 2016). However, at most locations around the world bathymetric surveys, or video imagery, of the surf zone covering a timespan of years to decades with sufficient temporal resolution are rare. Consequently, investigations on the long-term dynamics of crescentic sandbars are by necessity restricted to sites with sufficient data availability.

The increasing availability and accessibility of (free) multispectral satellite imagery offers an alternative dataset that can be used to investigate crescentic sandbar dynamics, also at locations where surveys or video imagery are unavailable. The images from the Landsat 4, 5, 7 and 8 missions provided by the United States Geological Survey (USGS) and National Aeronautics and Space Administration (NASA), and the images from Sentinel 2 mission provided by the European Space Agency (ESA) are freely available and accessible through the Google Earth Engine (GEE) platform (Gorelick et al., 2017). These images are globally available and have a spatial resolution (pixel size) of 30 m (for the Landsat missions) and 10 m (for Sentinel). The temporal resolution is in the order of days to weeks (depending on concurrent satellite missions) and the temporal extent is in the order of decades (e.g. imagery is available since the 1980s). Due to their spatial and temporal resolution and extent, these images can potentially be used to study medium to long-term (i.e. decadal) beach dynamics at any location in the world, where the sandbar alongshore variability is larger than the pixel resolution (i.e. 10 m for Sentinel or 30 m for Landsat imagery). However, applications of satellite imagery to date have been mainly restricted to shoreline extraction (Pardo-Pascual et al., 2012; Almonacid-Caballer et al., 2016; Hagenaars et al., 2018).

The aim of this paper is to explore the suitability of sandbar locations extracted from satellite images to investigate decadal scale crescentic sandbar dynamics with a focus of possible engineering applications based on a case study at Anmok beach in South Korea (Fig. 1). This paper is structured as follows: Section 2 describes the methods used for the sandbar crest line location extraction, its validation and its application to analyse decadal scale sandbar dynamics. Section 3 demonstrates the accuracy of the presented extraction technique in detecting the sandbar crest lines at the case study site compared to in situ data. Subsequently, the sandbar crest lines obtained are used to study the sandbar characteristics, migration rates and effects of human interventions at Anmok beach. The paper is concluded with a discussion in Section 4 followed by conclusions in Section 5.

2. Methods

2.1. Study site and data availability

Anmok beach is a straight, almost 4 km long wave dominated beach located on the East coast of South Korea, with waves predominantly incident from the northeast. The area is governed by a micro-tidal environment with tidal range of 0.1 to 0.3 m between neap and spring tide. Anmok beach is constrained in the south by the fishing port of Gangneung and in the north by a small stream that discharges from the Gyeongpo Lake (Fig. 1). The construction of Gangneung port started in 1996 and finished at the end of 2006. In 2014 a submerged breakwater (SBW) was constructed adjacent to the port, with a length of roughly 250 m and a crest level of 0.5 m below MSL.

The nearshore bathymetry is characterized by crescentic bars (Fig. 2), which is a typical feature along the South Korean East coast. The beach consists of medium to coarse sand, with a non-uniform distribution in the cross-shore direction (finer sand offshore) and an average grain size of 400 μm. The barred profile has a mild slope (~1/50) on average. At present, 14 bathymetric surveys that cover all or a part of Anmok beach with a spatial resolution of roughly 5 × 50 m (cross-shore × alongshore) are available. These surveys were performed mainly during 2007–2008 (4 surveys) and 2013–2015 (10 surveys) using RTK-DGPS for dry beach and single-beam echo sounders for submarine topography. Furthermore, 3 high quality (pixel size 0.5–1 m) aerial images are available from 1990 to 2005 and 9 panchromatic satellite images with a resolution of 1 m and 7 m from the Korean Satellites Arirang 1 and 2, respectively, are also available from 2000 to 2014.

The length scales of the sandbar patterns and the depth at the sandbar crest line were estimated from the available surveys. The mean value of the alongshore length of the crescents was equal to 390 m with a standard deviation of 160 m. The cross-shore length scales (i.e. distance from bay to adjacent horns) of the crescents has a mean value of 64 m with a standard deviation of 35 m. The average water depth at the

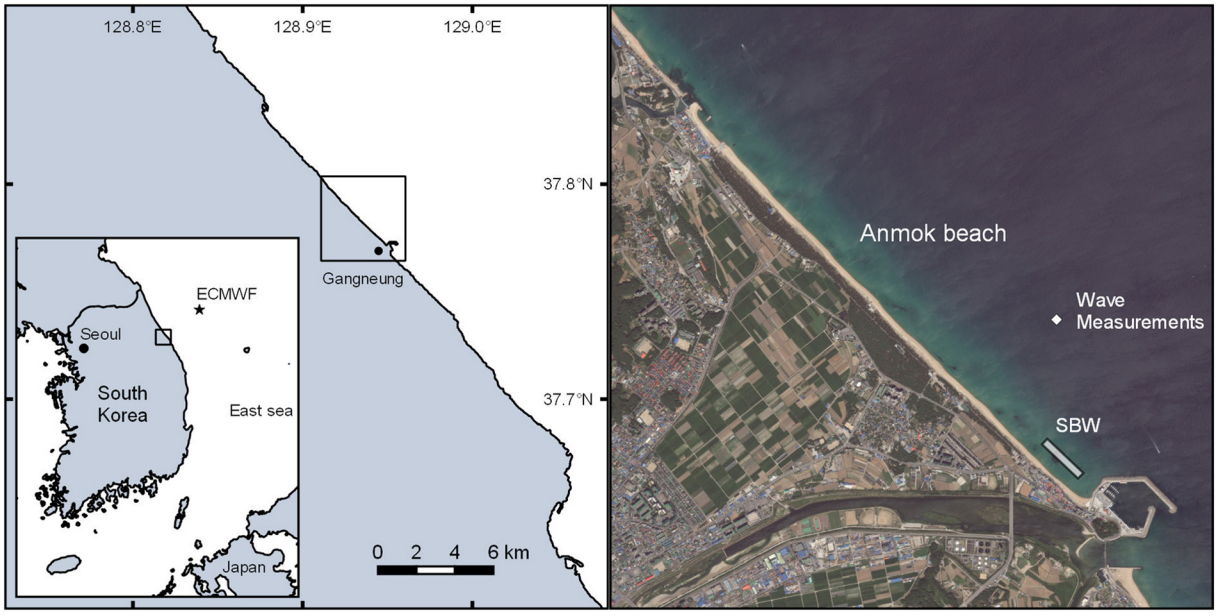

Fig. 1. Map showing the location of Anmok beach at the East coast of South Korea, at the city of Gangneung in Gangwon Province. The white indicator in the right panel shows the location of the wave measurements, while the asterisk in the left panel shows the location of the ECMWF grid point considered. The footprint of the SBW is indicated by the grey rectangle (Right panel aerial image obtained from Bing).

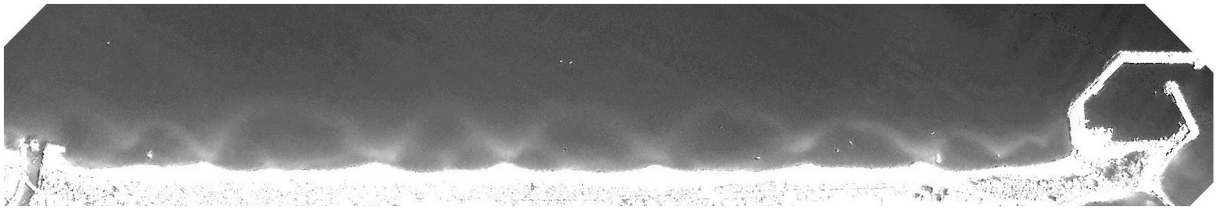

Fig. 2. Satellite image from the Korean Arirang 2 satellite, showing the panchromatic band at 23/11/2008. The crescentic sandbar features are visible by the whitish pixels indicating shallow areas.

horn locations was 3.1 m, while at the bay locations it was 4.3 m.

Wave conditions time series were available at a location 60 km offshore (Fig. 1), obtained from the ERA-Interim reanalysis (Dee et al., 2011) from the European Centre for Medium-Range Weather Forecasts (ECMWF) for the period between 1979 and end of 2016. The wave climate at Anmok can be characterized as relatively mild, with significant wave heights below 1.5 m during almost 80% of the time. The wave climate has a seasonal character with larger waves ($\overline{H_s} \approx 1.4\,m$) incident from the N-NE sector between September and February, while smaller waves ($\overline{H_s} \approx 0.8\,m$) incident from the NE-E sector between March and August (Fig. 3), except for occasional typhoons making landfall along the East coast. Wave measurements at Anmok beach were available between February 2015 and January 2016 at a location 800 m offshore at a depth of about 18 m, which were collected by a wave and current-profiler system (Fig. 1).

The wave conditions were transformed from offshore to nearshore for a set of 250 wave scenarios using a SWAN model (Booij et al., 1999). Based on the model simulations, statistical relationships have been derived between the offshore and nearshore wave parameters and stored in a transformation matrix (van Os and Caires, 2011). Using this matrix the entire 27 years offshore time series could efficiently be transformed into nearshore time series (i.e. at the location of the local wave measurements), by means of interpolation of each wave condition in the time series based on the available wave conditions in the matrix. The nearshore time series of wave conditions thus obtained were compared with the wave measurements collected, which indicated some bias between modelled and measured wave conditions. In order to correct the observed bias, the slopes of the regression lines were used to correct the modelled values of the nearshore wave heights. After the correction, the correlation coefficient r between the modelled and observed significant wave heights (H_s) was 0.92, while the RMSE was 0.26 m. The thus obtained nearshore wave conditions were used to study the sandbar dynamics with respect to wave forcing and to neglect high wave energy periods from the validation procedure of the satellite derived sandbar crest lines against in-situ surveys.

2.2. Extraction of sandbar position from satellite images

Satellite images from the Landsat 5, 7, 8 and Sentinel 2 missions were obtained for the study area for the period of 1990–2017 using the GEE platform (Gorelick et al., 2017), using a threshold of 25% for cloud coverage at the study area to preliminary exclude images with high cloud density. Each of the obtained images was inspected in true colour format, in order to visually estimate the sandbar crest line location (Fig. 4). The visual estimation was performed by locating the difference of the pixel colour intensity at the shallow areas of the sandbar crest, creating data points of the location coordinates. In a large number (~65%) of the available images the sandbar detection was hampered by image quality or the presence of clouds and wave breaking (foam). Excluding these images resulted in 175 images of sufficient quality to visually detect the sandbar crest lines.

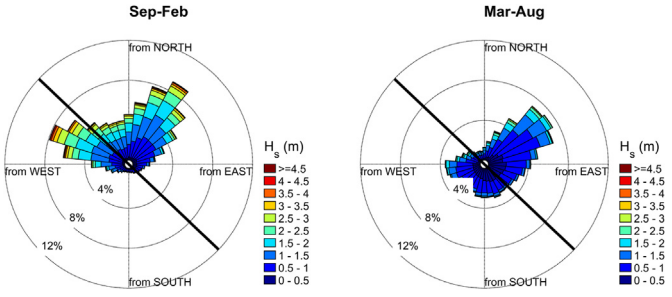

Fig. 3. Wave roses of significant wave height (H_s) at the ECMWF offshore grid point location (Fig. 1) for the periods of September to February (left) and March to August (right). Thick black line indicates the orientation of the coastline at Anmok beach.

For each mission the satellite images available on the GEE platform were georeferenced with respect to the first image of the image collection. However, the missions were not necessarily georeferenced with respect to each other and in-situ data. Therefore, each image in each collection was geometrically corrected. The geometric correction was performed using 8 Ground Control Points (GCP) on one image from each collection (García-Rubio et al., 2015; Shen et al., 2017). The selected GCPs were defined by the centroids of large (non-moving) natural or human made ground features, like large lakes and ports. The GCPs were defined several times by the same user indicating sub-pixel errors between the different tries. It is expected that since the ground feature edges are quite distinct, the same magnitude of errors, will most likely apply if different users define the same GCPs. For the correction of the patterns and images, an affine transformation was used. The resulting root mean square error (RMSE) between the corrected image and the GCPs was 6.5, 8, 4 and 3 m for the Landsat 5, 7, 8 and Sentinel 2 respectively. For all the image collections the RMSE was significantly smaller than the pixel size (i.e. 30 m for Landsat and 10 m for Sentinel) and, therefore, considered sufficiently small for the purpose of this study.

Each of the 175 observations was transformed to the local coordinates of Anmok beach, with the origin defined by a point next to Gangneung port and the orientation of the coastline. This defined a reference line, from which the cross-shore location of the sandbar was calculated (i.e. x = 0 line in Fig. 4). Afterwards, the data points were interpolated on an alongshore 5 m grid and smoothed with a 50 m window moving-average filter. The choices for the grid size and the filter window were based on a sensitivity analysis and are further discussed in Section 4. This procedure resulted in a vector $x_b(y)$ of sandbar cross-shore crest line positions at alongshore locations y, for each available observation in time (Fig. 4).

2.3. Validation of satellite derived sandbar location

In order to evaluate the accuracy of the extracted sandbar locations, the sandbar crest lines were compared with available bathymetric surveys at Anmok beach. The number of concurrent satellite images and bathymetric surveys was limited. Therefore, the images taken closest to the dates of the bathymetric surveys were selected. In order to minimize the risk of significant morphological changes having occurred between the date of the image and the survey, the selection of images was further constrained to a maximum time difference of 30 days with no

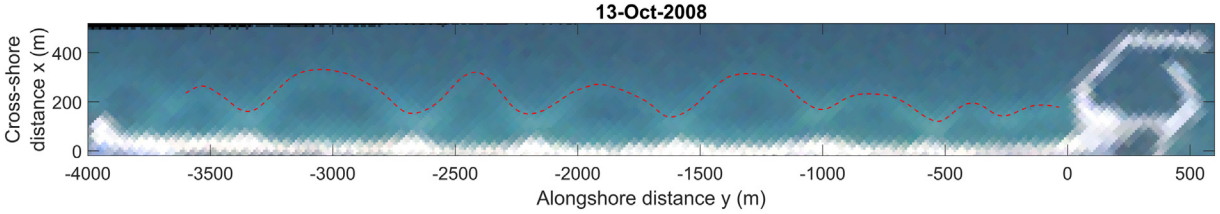

Fig. 4. Sandbar crest line location xb(y) at Anmok beach detected from a satellite image from the Landsat 8 mission.

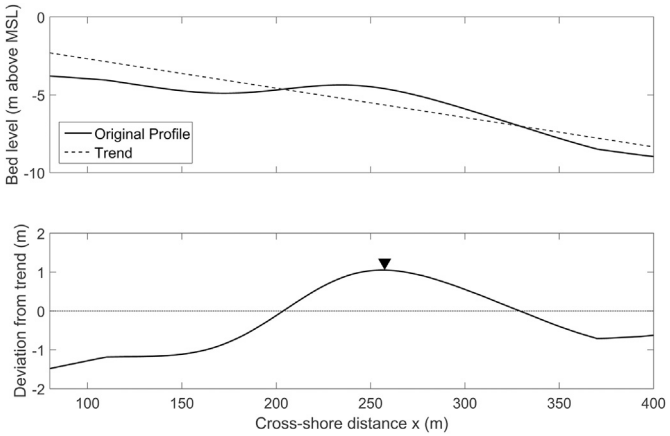

Fig. 5. Estimation of bar crest location for the profile at the alongshore location y = −1780 m for the survey of October 2008. Top panel: Original profile and alongshore-averaged slope of survey. Bottom panel: Bed level deviation from trend and crest line location represented by the triangle.

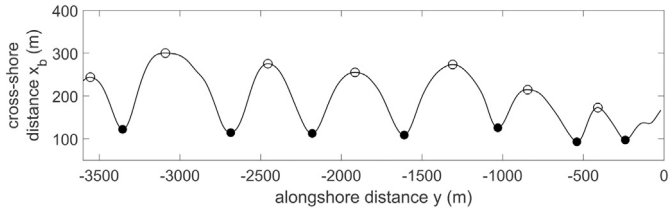

Fig. 6. Example of detection of horns (filled circles) and bays (open circles) for the sandbar crest line at 13th of October 2008.

severe wave events (H_s < 2.5 m) occurring in between. The wave height threshold was chosen after testing different values in order to avoid significant morphological changes between the date of the survey and the date of the image, while maintaining a realistic number of surveys for the validation. This resulted in 9 pairs of sandbar patterns for the validation. It is noted that all of the selected images were from Landsat missions, which have a pixel resolution of 30 m.

The bar crest line for each survey was computed by detecting the elevation peak in the detrended cross-shore profiles with a spacing of 5 m in the alongshore direction (Fig. 5). The trend was computed as the slope of the alongshore-averaged cross-shore profile for each survey. Furthermore, in order to deal with noise in the survey data and produce a continuous sandbar crest line, the bathymetry was smoothed using a moving average filter with a window of 30 m in both directions. The moving average window was selected based on a sensitivity analysis. For the available surveys at Anmok beach the 30 m window gave a continuous crest line while maintaining the sandbar variability.

2.4. Derivation of sandbar characteristics and dynamics

From each sandbar crest line position $x_b(y)$, the bays and horns were detected as local minima and maxima respectively, with a restriction of a minimum 5 m cross-shore distance between them to avoid the detection of small perturbations as crescents (Fig. 6). Each crescent was defined by two successive horns and an intermediate bay. The alongshore and cross-shore length scales were computed based on van Enckevort et al. (2004). The amplitude A of each individual crescent was defined as half the mean cross-shore distance between the bay and the two adjacent horns and the wavelength L as the alongshore distance between the horns. In each individual observation in time the crescent characteristics were averaged over the alongshore direction to provide the alongshore mean values $\overline{A}$ and $\overline{L}$. Additionally, the alongshore mean cross-shore location of the sandbar $\overline{x_b}$ was computed with respect to the reference line for each of the available observations. In order to measure the alongshore variability of the sandbar, the standard deviation of the sandbar crest line from its alongshore mean cross-shore location std(x_b) was calculated for each observation.

In order to highlight the sandbar features (bays and horns), a 5th order polynomial fit was removed from each observation $x_b(y)$, following Van de Lageweg et al. (2013). Different order polynomials were tested (1st–6th), but the 5th order polynomial was the one that performed best in capturing the large-scale parabolic shape of the sandbar and highlighting the sandbar features. This results in the perturbation vector $x_{b5}(y)$, which describes the sandbar perturbations from its (alongshore variable) mean position.

In order to study the sandbar alongshore migration the sandbar patterns in consecutive observations were assumed to have similar characteristics. This allowed for the calculation of the mean alongshore migration of the sandbar features by cross-correlating consecutive sandbar perturbation observations $x_{b5}(y)$. The mean alongshore migration distance of the sandbar patterns was calculated as the lag at the positive peak closest to the origin of the cross-correlogram (van Enckevort et al., 2004). The sign of the lag indicated the migration direction, with positive lags representing migration to the northwest.

Human interventions, such as ports, may affect sandbar characteristics. As described in Section 2.1, the Gangneung port was constructed between 1996 and 2006, where the port's northern breakwater reached its most offshore location in 2000. To study the effects of the port's construction at Anmok beach, the characteristics of the sandbar were compared both in time, by comparing the characteristics of the sandbar between two 10 year periods before and after the port construction (i.e. 1990–2000 and 2000–2010) and in space, by identifying the beach area that was affected by the port construction. This area was estimated by comparing the sandbar length scales in the alongshore direction for the two predefined periods.

3. Results

3.1. Accuracy of satellite derived sandbar crest lines

Visually, the sandbar location detected from satellite imagery and surveys were in good agreement (Fig. 7). In order to quantify the accuracy of the extraction method, the RMSE between the in-situ and satellite derived sandbar cross-shore location was calculated for each of the 9 pairs. The RMSE was ranging from 14.6 to 21.3 m with an average of 17.6 m. For all pairs the error was well within the pixel resolution of the satellite images (30 m). This provides sufficient confidence in the extraction method and the accuracy of the detected bar patterns. In

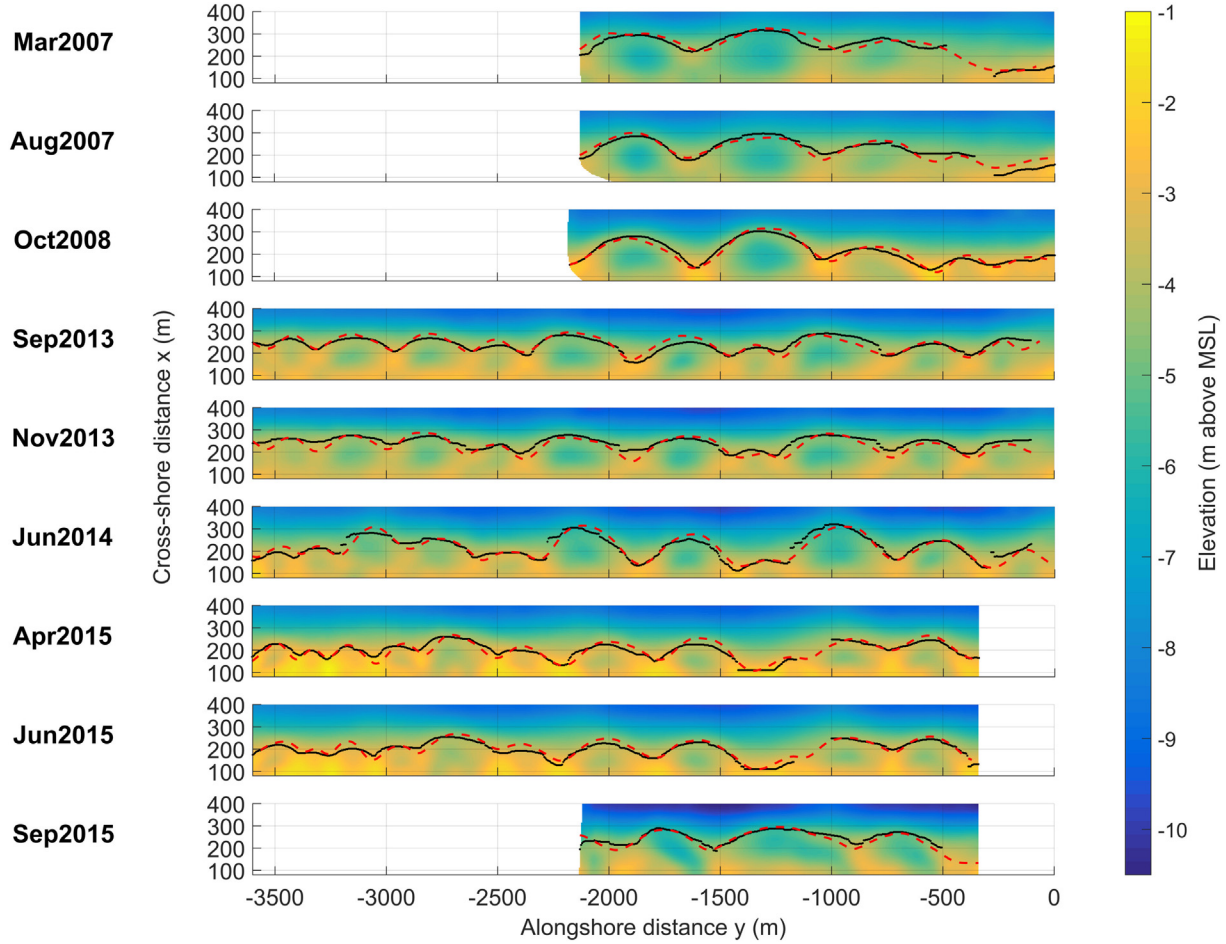

Fig. 7. Bathymetries at Anmok beach from 9 available surveys. The colour scale indicates the elevation of the bed level w.r.t to MSL. Red dashed lines show the sandbar crest-line location estimated from the satellite images. Black lines show the sandbar crest line detected from the bathymetric surveys. The area affected by the construction of the Anmok submerged breakwater (SBW) from October 2014 is omitted from this figure ($-350\,\text{m} < y < 0\,\text{m}$). The reader is referred to the web version of this paper for the colour representation of this figure. (For interpretation of the references to colour in this figure legend, the reader is referred to the web version of this article.)

order to validate that there was no systematic error in the detection of the sandbar crest line using the proposed technique, the bias between the satellite and survey derived sandbar crest lines was calculated for each of the available observations. The average bias over the 9 available observations was $-0.35\,\text{m}$ with a minimum and maximum value of -13.1 and $7.7\,\text{m}$ respectively. This highlights that there was no systematic error present. It is noted that the estimation error of the presented technique comprises both errors arising from satellite sensors capacity to resolve the sandbar features and human subjectivity in detecting the sandbar crest line.

3.2. Sandbar characteristics and dynamics

The previous section demonstrated that crescentic sandbar patterns extracted from satellite imagery are similar to those obtained from field measurements. Using this technique increased the number of available observations at Anmok beach significantly from 26 without to 201 with free satellite imagery within the period 1990–2017 (Fig. 8). Plotting the sandbar cross-shore position $x_b(y)$ for all of the available observations at Anmok beach provides an overview of the sandbar patterns and dynamics over the study period (Fig. 9). The temporal resolution of the observations ranged from one day to almost a year, depending on the satellite revisit time, the total number of satellite missions per period and the image quality (clouds or non-detectable sandbars). The average time interval between consecutive observations was 1.5 months.

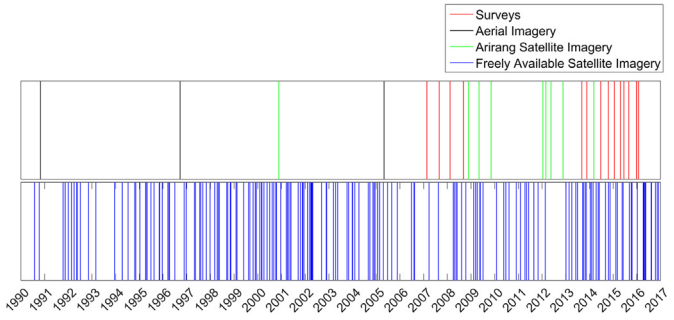

Fig. 8. Observations at Anmok beach through the study period from different sources.

At the instants of the available observations during the study period (1990–2017) the sandbar always showed an alongshore rhythmic (crescentic) shape, with various crescents forming in the alongshore direction. It appears that through the years the sandbar migrated both in the alongshore and cross-shore direction, but preserved its overall shape. The only abrupt change of the sandbar position took place at the end of 2015, when typhoon Goni made landfall on the South Korean East coast, with H_s reaching 5.5 m, followed by a stormy period that lasted for almost one month. During this period the sandbar moved on average offshore (i.e. increase of $\overline{x_b}$) and the standard deviation around

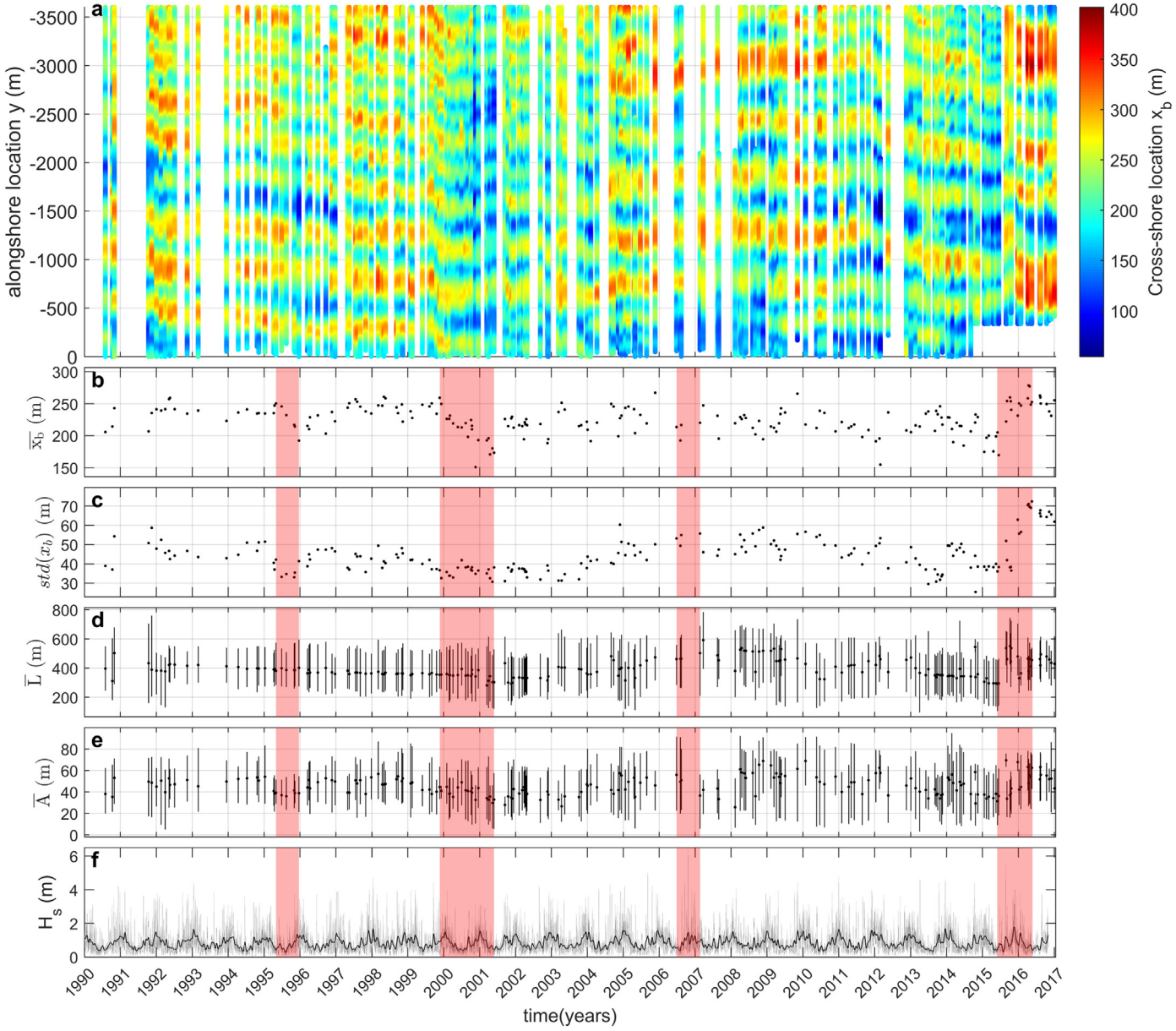

Fig. 9. a) Hovmöller diagram of the sandbar cross-shore locations x_b. Red colours indicate parts of the sandbar further away from the reference line while blue indicates parts that are closer to the reference line. The x-axis represents time in years while the y-axis shows the alongshore location of the sandbar measured from Gangneung port. White gaps indicate periods when no data are available or the omitted area around the Anmok SBW. Observations of b) the alongshore mean cross-shore location of the sandbar $\overline{x_b}$, c) the standard deviation of the sandbar crest line from its alongshore mean cross-shore location std.(x_b), d) alongshore mean crescentic wavelength $\overline{L}$ (with vertical line indicating minimum and maximum values), e) alongshore mean crescentic amplitude $\overline{A}$ (with vertical line indicating minimum and maximum values) and f) time series of significant wave height H_s at the nearshore (grey line) and the 15 days average of H_s (black line). The highlighted red areas indicate periods of interest that are discussed in this section. The reader is referred to the web version of this paper for the colour representation of this figure. (For interpretation of the references to colour in this figure legend, the reader is referred to the web version of this article.)

its mean cross-shore location std.(x_b) increased. After typhoon Goni, phenomenological merging (i.e. individual crescents merging into one) took place, with the average wave length of the crescents $\overline{L}$ almost doubling from 290 m to 550 m. On the other hand, after the winter season, when H_s was lower, the average wave length became smaller again. This is in line with Van Enckevort et al. (2004), where the authors observed that merging phenomena are mostly connected with an increase in wave height, while splitting phenomena (i.e. one crescent splitting into multiple) take place during a decrease in H_s. During an extreme storm at the end of 2006 (when peak H_s reached 6 m) the alongshore average crescentic amplitude $\overline{A}$ dropped from 50 m to 35 m, but $\overline{x_b}$ remained stable. It is noted that during this winter season there were no observations available between the pre- and post-winter period (i.e. five months gap), hence there was no data to analyse the actual response of the sandbar during the storm.

Two other periods that are highlighted in Fig. 9 are the second half of 1995 and the period covering the year 2000 and the first half of 2001. During these periods the sandbar migrates onshore (i.e. indicated by a decrease of $\overline{x_b}$), while the length scales of the sandbar patterns remain relatively stable. It can be observed that during these periods there were no extreme storms ($H_s > 4$ m) hitting the South Korean East coast.

Fig. 10 shows the probability distributions for the sandbar characteristics in terms of $\overline{x_b}$, A and L over the study period, with and without the additional observations from the freely available satellite imagery (SI). When including the SI observations, the mean value of the

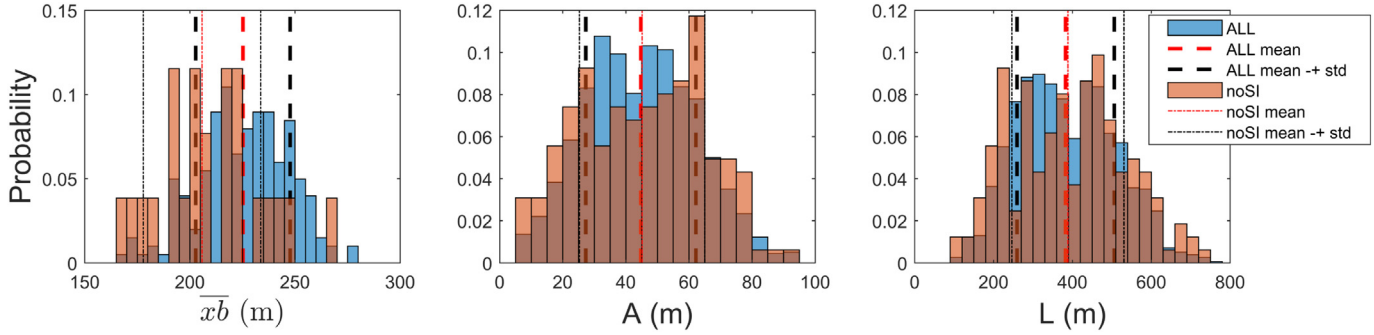

Fig. 10. Probability distributions of: (left) alongshore-mean cross-shore location of sandbar $\overline{x_b}$ for each sandbar pattern in time, (centre) amplitude A of the individual crescents and (right) wavelength L of the individual crescents. The dataset with the satellite image observations included (ALL) and with only the locally available data (noSI) are presented by the bars with the blue and orange colour respectively. The red dashed lines represent the mean value, while the black dashed lines indicate the values within one standard deviation from the mean. The bin resolution is 5 m for $\overline{x_b}$ and A, and 40 m for L. The reader is referred to the web version of this paper for the colour representation of this figure. (For interpretation of the references to colour in this figure legend, the reader is referred to the web version of this article.)

alongshore averaged cross-shore location of the sandbar $\overline{x_b}$, for the 201 sandbar observations was 225 m while its standard deviation was 23 m. Through the study period, 1541 individual crescents were detected at Anmok beach. Both the amplitude A and the wavelength L of the crescents presented a distribution that showed 2 peaks; for the amplitude A at 30 m and 50 m and for the wavelength L at 300 m and 450 m. These peaks can be connected with the difference of the average length scales between the crescents at the SE and NW part of the beach. For the amplitude A, the mean and standard deviation values were 45 m and 18 m, while for wavelength L they were 383 m and 123 m respectively.

When only the locally available data were used (i.e. no SI observations), the probability distributions of the sandbar characteristics significantly diverged from the ones that included the SI observations (Fig. 10). Due to the low number of observations, the distributions contain a number of peaks. However, the mean and standard deviation of the amplitude and wave length were quite similar to those when the SI observations were included. This similarity of the two datasets can be connected with the amplitude and length characteristics of the crescents at Anmok beach, which respond to forcing slowly during the study period (Fig. 8). On the other hand, for the mean cross-shore location of the sandbar, the mean value was located 20 m shorewards with respect to the value when the SI observations were included. These results indicate that the added value of the extra sandbar observations is directly connected with the dynamics of the sandbar system under study (i.e. in a more dynamic system the added value will be higher).

3.3. Alongshore sandbar migration

Plotting the cumulative alongshore migration of the sandbar (Fig. 11) during the study period shows that there were long-term trends in the alongshore migration direction, with seasonal variations, likely due to the seasonal character of the incoming wave direction (Section 2.1). Fig. 11 indicates that the sandbar migrated almost 600 m to the southeast between 1990 and 2004, while from 2004 to 2007; the sandbar migrated in the opposite direction by almost 200 m. After 2007, the sandbar migrated again to the southeast by almost 350 m until the summer of 2015, at which time typhoon Goni made landfall at the East coast and a large migration to the northwest was observed during August 2015, in accordance with observations of wave direction during the typhoon being predominately from the NE-E sector (Athanasiou, 2017). It may be argued that a reset (or partial reset) event might have occurred between the typhoon's attack and the first available observation afterwards. A reset event describes a situation, when under high energy wave conditions, the prevailing alongshore rhythmicity of a sandbar is reworked by wave action into an essentially alongshore uniform sandbar (de Schipper et al., 2011; Smit et al., 2011; Blossier et al., 2012). As a reset event is usually present for a very small amount of time in the order of 1 or 2 days (Ranasinghe et al., 2004; van Enckevort et al., 2004; de Schipper et al., 2011), it may have not been captured by the available observations, thus rendering any connection between the two sandbar patterns meaningless. This is further discussed in Section 4.

3.4. Structural impacts on sandbar characteristics

The amplitude A and wavelength L of the individual crescents detected at Anmok beach show an alongshore trend, with longer length scales appearing in the area $-2000\,\text{m} < y < -600\,\text{m}$ and smaller length scales at the north-western side of the beach (Fig. 12). Comparing the sandbar characteristics at all the alongshore extent for the two periods before and after the port construction (i.e. 1990–2000 add 2000–2010 respectively) indicates that both A and L close to the port have become on average smaller after the port construction (Figs. 12 and 13). The amplitude and wavelength in an area 650 m away from the port have decreased on average by 33% and 22% respectively. Assuming independent groups for each sample, before and after the port construction, a 2-sample *t*-Test was performed and these differences were found statistically significant for both A and L. In order to verify that this change was not part of the temporal natural variability of the sandbar at Anmok, the same statistics were computed for the rest of the beach area (Fig. 13). The differences between the average A and L farther away from the port were 3% and 4.5%, respectively. These changes are negligible and indicate that the changes closer to the port are very likely to be connected to the port construction.

It is likely that this kind of sandbar response adjacent to a port is connected with the shadow zone that is created in the lee of the port's breakwater during specific conditions. This is because the wave heights and currents in this area are significantly diminished due to the sheltering effect of port breakwaters, which may in turn damp the morphodynamics of the sandbar. The results of this section regarding the decrease of the sandbar characteristics next to the port are in agreement with the results from Bouvier et al. (2017), where the sandbar is linearized (smaller rhythmicity and amplitude A) in response to the construction of an offshore submerged breakwater.

4. Discussion

4.1. Accuracy and applicability

In the present study freely available satellite images were used to manually extract the sandbar position over time at Anmok beach. To be able to use this technique at other locations, the sandbar cross-shore

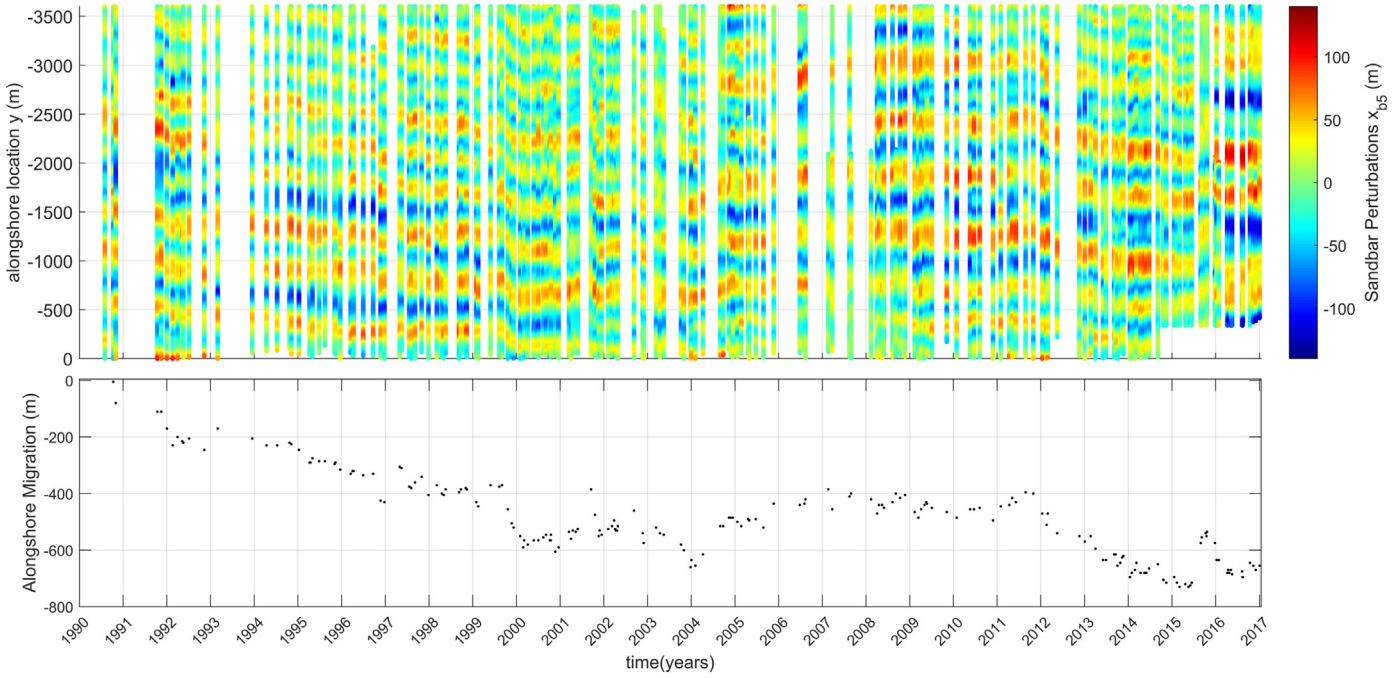

Fig. 11. (top) Hovmöller diagram of the sandbar perturbations $x_{b5}(y)$ from its mean position. Blue colours describe shoreward perturbations (horns) while red colours describe seaward perturbations (bays). The vertical axis shows the alongshore location of the sandbar measured from Gangneung port. The horizontal axis shows the time in years. White gaps indicate periods where no data are available or the area of the SBW which was omitted. (bottom) Alongshore cumulative migration of the sandbar features for the study period. The reader is referred to the web version of this paper for the colour representation of this figure. (For interpretation of the references to colour in this figure legend, the reader is referred to the web version of this article.)

perturbations must have sufficiently large length scales in relation to the image pixel resolution to be detected from satellite imagery. At Anmok beach the amplitude of the crescents was generally in the order of 40 m, translating to an 80 m horn to bay variation. This was sufficient to visually identify the sandbar cross-shore perturbations from the 30 m resolution Landsat satellite imagery as was shown by the validation with in-situ surveys (Section 3.1). At locations where the sandbar variations are smaller (e.g. < 30 m), the Landsat spatial resolution (30 m) will not be adequate to visually extract the sandbar crest location, with the error (RMSE of 17.6 m) being large compared to the length scales of the sandbar crescentic characteristics, to provide confidence in the results. In the present study the sandbar crest line that was extracted manually from the satellite images was first interpolated on a 5-m alongshore grid, which was big enough to capture the sandbar horizontal features at Anmok beach. Then it was smoothed in the alongshore direction using a moving average filter with a window of 50 m.

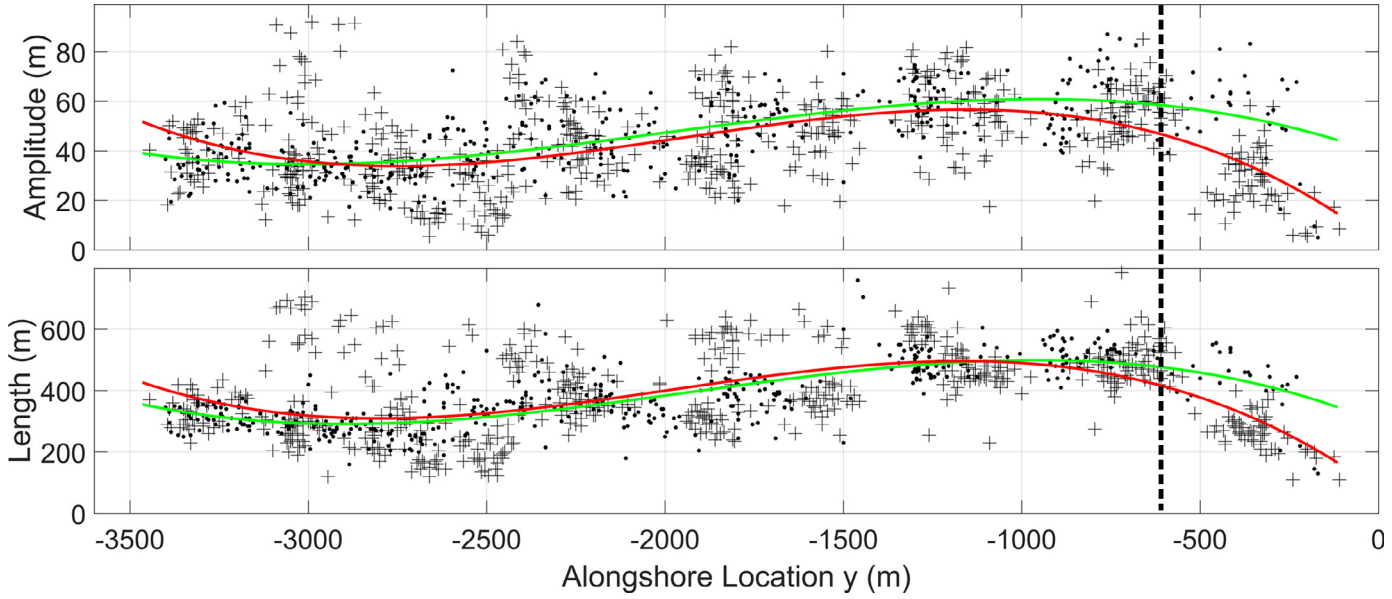

Fig. 12. Amplitude A and wavelength L of the individual crescents detected at Anmok beach in the periods of 1990–2000 (dots) and 2000–2010 (crosses), describing the pre- and post-port situation respectively. The green (red) line is the best cubic fit of the pre (post) port period data. The vertical dashed line indicates the alongshore distance from the port, where the differences between the two periods are most pronounced. The reader is referred to the web version of this paper for the colour representation of this figure. (For interpretation of the references to colour in this figure legend, the reader is referred to the web version of this article.)

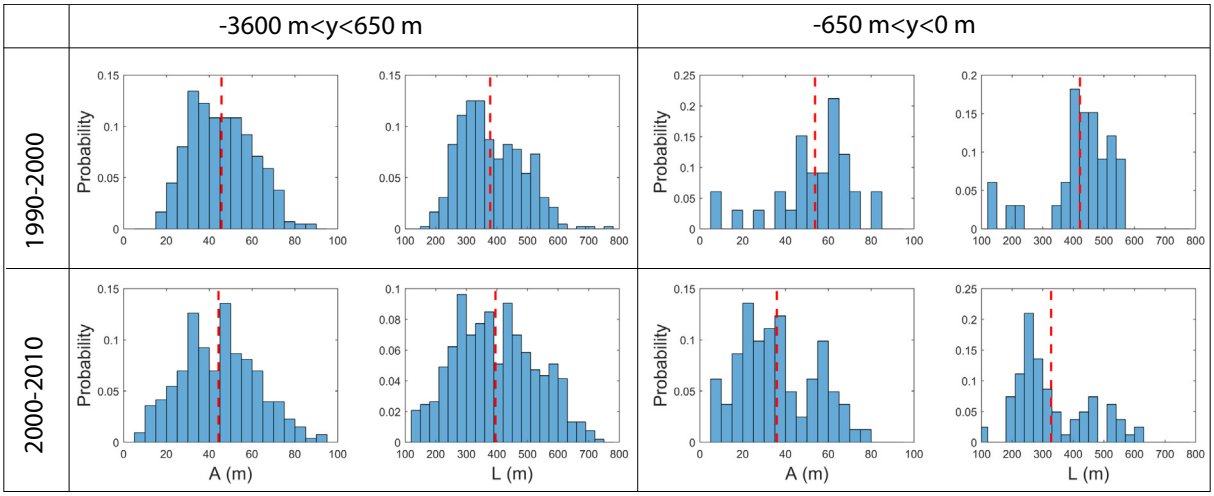

Fig. 13. Amplitude (left) and length scale (right) histograms of the individual crescents for the pre- (1990–2000) and post- (2000 − 2010) port periods, for the areas $-3600\,m < y < -650\,m$ and $-650\,m < y < 0\,m$. Red dashed line indicates the mean value. The reader is referred to the web version of this paper for the colour representation of this figure. (For interpretation of the references to colour in this figure legend, the reader is referred to the web version of this article.)

Different windows were tested in order to ensure that noise caused by the manual extraction was filtered from the final sandbar crest line, while the alongshore variability is maintained. For other case studies, the choice of the filtering window should be based on the site-specific length scales of the crescents. At locations with smaller length scales, a smaller window will be necessary to maintain the alongshore variability.

Water clarity is another important factor that governs the feasibility of the sandbar extraction technique presented in this paper. In areas with turbid waters the estimation of the sandbar location from satellite images may be difficult or even impossible. In locations where the sandbar is more dynamic and responds faster to wave forcing, the temporal resolution of the satellite imagery (in comparison to video techniques) may restrict the comprehensive study of sandbar dynamics. Large temporal gaps in between the observations can possibly mask its dynamics. This should be taken into account when calculating alongshore migration rates of the sandbar patterns as well.

The increasing temporal resolution of the freely available satellite images and the higher spatial resolution of Sentinel 2 mission will increase the potential of their application to derive sandbar characteristics. The pixel resolution of Sentinel 2 (10 m) is likely to decrease the RMSE of the sandbar manual extraction technique to smaller values than the 17.6 m found for the Landsat imagery in the present study. This can increase the applicability of this technique to areas with moderate sandbar cross-shore perturbations (e.g. A∼10–20 m). With Landsat 7 and 8 and Sentinel 2 being in orbit at present the temporal resolution of the available satellite images is already increased, while Landsat 9 is planned for launch in 2020 (Markham et al., 2016), which will further increase the number of available observations.

In this study a manual extraction technique was used to extract the sandbar position from satellite imagery, which is a labour intensive task. Automated techniques could possibly speed up this procedure. We attempted to use automatic techniques to derive the sandbar location based on the pixel intensity. However, the results were not satisfactory, as in some cases the automatic detection algorithm failed to identify distinct intensity peaks and in cases where intensity peaks were detected the extracted sandbar crest lines deviated extensively from the real position when compared with the available surveys (i.e. mean RMSE of 40 m). This is possibly connected to the spatial resolution of the Landsat imagery (30 m), sun glint effects, foam induced by wave breaking or the differences in the absorption and scattering of light due to particles present in the water column. With increasing image resolution and foreshadowed improvements in the satellite sensors, automated detection of the sandbars may be possible in the near future.

This study showed that the additional sandbar observations obtained from satellite images can be used to study long-term (decadal) sandbar characteristics, dynamics and impacts of human interventions. For other case studies the sandbar observations from satellite images may also contribute in providing qualitative (historic) validation data for medium-term (weeks-year) process based modelling efforts and training datasets for empirical models (Plant et al., 1999, 2006; Pape et al., 2010; Splinter et al., 2011) geared for simulating interannual sandbar migration.

4.2. Sandbar-shoreline coupling

The timespan that was studied for the Anmok case is 1990–2017. Sentinel imagery (with a pixel resolution of 10 m) is only available since 2015, which restricted the availability of satellite images mainly to Landsat images (with a pixel resolution of 30 m). This did not allow us to study the relatively moderate coastline patterns (i.e. maximum cross-shore perturbations of 20–30 m) at Anmok beach using satellite imagery on a decadal time scale. Nevertheless, using available GPS shoreline measurements and manually derived shorelines from the Sentinel 2 and the Korean Arirang satellite missions, we generated 46 pairs of sandbars and shorelines at Anmok beach from 2008 to 2017. As the number of observations was sparse from 2010 to mid-2015, only two periods were studied. The period between mid-2008 and end-2009 encompasses shoreline observations from GPS measurements and Korean satellites. The period from mid-2015 to end 2016 encompasses mainly shoreline observations from the Sentinel 2 mission. The coupling (or no coupling) between the sandbar and the shoreline was measured with the cross-correlation function r, which has been previously employed to calculate the coupling between inner and outer sandbars at different spatial lags (Ruessink et al., 2007a; Price and Ruessink, 2013). The test for statistically significant non-zero correlation was performed using the method outlined in Garrett and Toulany (1981). Additionally, the separation of the sandbar and shoreline was measured as the distance between the mean cross-shore position of the sandbar and the mean cross-shore position of the shoreline. During the first period (2008–2009) all seven sandbar-shoreline observations were found to present significant coupling (at the 95% confidence level) with a negative cross-correlation and an average value of $\bar{r} = -0.65$. On the other hand, during the second period (2015–2016) only half of the 14 observation presented significant coupling, with all seven of them having a positive cross-correlation and an average value of $\bar{r} = 0.46$.

The negative r values of the first period indicate out of phase coupling while the positive ones of the second period express an in-phase coupling. Out of phase coupling describes a situation, where the sandbar horns (i.e. onshore perturbations) are faced by shoreline horns (i.e. offshore perturbations) and the sandbar bays (i.e. offshore perturbations) are faced by shoreline bays (i.e. onshore perturbation). During the first period the coupling between the shoreline and sandbar was on average stronger, which can be connected with the smaller separation in comparison to the second period (i.e. 190 m vs. 230 m), in which high energy storm events have taken place. Nevertheless, a low correlation coefficient does not necessarily imply that the sandbar and shoreline were not connected, as a diverse alongshore response with high positive and high negative correlation at different beach sections, can lead in overall values close to zero. Previous studies focusing on sandbar and shoreline coupling have shown similar results (Van de Lageweg et al., 2013). With the growing Sentinel 2 imagery dataset, it will become possible to extract concurrent sandbar and shoreline patterns for longer time periods, enabling the investigation of their coupling at locations around the world. This can extend the capacity of the technique presented in relation to coastal zone management applications.

4.3. Anmok sandbar patterns

The wavelengths of crescentic sandbars around the world have been found to vary extensively, with values ranging from 100 to 3000 m (van Enckevort and Ruessink, 2003). The wavelengths found at Anmok beach, ranging from 100 to 800 m with a mean value of 390 m, resemble the length scales of case studies in Australia (Short, 1985), New Zealand (Brander et al., 1999), Japan (Homma and Sonu, 1962), Denmark (Aagaard, 1988) and the Netherlands (Ruessink et al., 2000). The results of the present study suggest that the sandbars at Anmok beach have a persistent pattern, which was altered only due to very intense and prolonged storm wave conditions (e.g. typhoon Goni and winter 2015–2016). This has been previously observed for the outer sandbar at Truc Vert Beach in France (Castelle et al., 2007), which demonstrated persistent crescentic patterns as well (with a mean wavelength of 700 m) and was inactive for $H_s < 3$ m. Our results with respect to the effects of the port construction at Anmok beach can be connected to the study of Rutten et al. (2018). In this study the authors concluded that the alongshore variability in wave height and direction induced by the curvature of the coast (caused by a large scale nourishment) results in differences in the sandbar length scales and response times. A human structure (like a port's breakwater or a groin) can induce a similar alongshore variability in wave characteristics and thus affect the sandbar characteristics as demonstrated in the present study.

5. Conclusions

Freely available satellite images were used to analyse long-term (decadal) sandbar dynamics at Anmok beach at the East coast of South Korea. Validation of the extracted sandbar locations from satellite imagery against 9 in-situ bathymetric surveys shows good agreement with an average RMSE of 17.6 m and no systematic bias. Using this freely available satellite imagery increased the total number of observations at Anmok beach from 26 to 201 within the study period 1990–2017. The applicability of the presented technique is dictated by the feasibility of the visual extraction of the sandbar crest line from the satellite imagery, which is in turn dependent on: (1) cross-shore crescentic length scales being larger than the image resolution, (2) absence of frequent wave breaking or clouds and (3) water clarity.

The additional sandbar observations enabled to study its decadal scale dynamics at Anmok beach. It was found that within the study period 1990–2017 the sandbar maintains a persistent pattern that is only altered during prolonged and very intense storm conditions. The increased temporal resolution of sandbar observations facilitated the investigation of the cumulative migration of the sandbars. The results show that the cumulative alongshore migration was in the order of hundreds of meters over the 27 years study period. The satellite imagery also considerably increased the number of observations before the construction of Gangneung port (i.e. from 2 to 57), which allowed for a comparison of sandbar characteristics before and after the port construction. The results indicate that both the amplitudes and wavelengths of the sandbar crescents near the port have decreased after its construction.

Acknowledgements

This paper is funded by the research project titled “Development of Coastal Erosion Control Technology (or CoMIDAS)” of the Korean Ministry of Oceans and Fisheries and the Deltares strategic research program Coastal and Offshore Engineering. This financial support is highly appreciated. Furthermore, the authors would like to thank the Korean Ministry of Oceans and Fisheries for providing the necessary survey data. RR is supported by the AXA Research fund and the Deltares Strategic Research Programme ‘Coastal and Offshore Engineering’. Additionally, we would like to thank the two reviewers whose comments and suggestions helped to greatly improve this manuscript.

References

Aagaard, T., 1988. Rhythmic beach and nearshore topography: examples from Denmark. Geogr. Tidsskr. J. Geogr. https://doi.org/10.1080/00167223.1988.10649257.

Almar, R., Castelle, B., Ruessink, B.G., Senechal, N., Bonneton, P., Marieu, V., 2010. Two- and three-dimensional double-sandbar system behaviour under intense wave forcing and a meso-macro tidal range. Cont. Shelf Res. 30, 781–792. https://doi.org/10.1016/j.csr.2010.02.001.

Almonacid-Caballer, J., Sánchez-García, E., Pardo-Pascual, J.E., Balaguer-Beser, A.A., Palomar-Vázquez, J., 2016. Evaluation of annual mean shoreline position deduced from Landsat imagery as a mid-term coastal evolution indicator. Mar. Geol. 372, 79–88. https://doi.org/10.1016/j.margeo.2015.12.015.

Athanasiou, P., 2017. Understanding the Interactions Between Crescentic Bars, Human Interventions and Coastline Dynamics at the East Coast of South Korea. Technical University of Delft.

Blossier, B., Brière, C., Roelvink, J.A., Walstra, D.J.R., 2012. Characterization of processes involved in the reset of a subtidal bar. Coast. Eng. Proc. 1 (33). https://doi.org/10.9753/icce.v33.sediment.101. sediment.101.

Booij, N., Ris, R.C.C., Holthuijsen, L.H., 1999. A third-generation wave model for coastal regions. I - model description and validation. J. Geophys. Res. 104, 7649–7666. https://doi.org/10.1029/98jc02622.

Bouvier, C., Balouin, Y., Castelle, B., 2017. Video monitoring of sandbar-shoreline response to an offshore submerged structure at a microtidal beach. Geomorphology 295, 297–305. https://doi.org/10.1016/j.geomorph.2017.07.017.

Brander, R.W., Short, A.D., Osborne, P.D., Hughes, M.G., Mitchell, D.M., 1999. Field measurements of a large-scale rip current system. Coastal Sediments '99 Vols 1–3.

Caballeria, M., Coco, G., Falqués, A., Huntley, D.A., 2002. Self-organization mechanisms for the formation of nearshore crescentic and transverse sand bars. J. Fluid Mech. 465, 379–410. https://doi.org/10.1017/S002211200200112X.

Castelle, B., Bonneton, P., Dupuis, H., Sénéchal, N., 2007. Double bar beach dynamics on the high-energy meso-macrotidal French Aquitanian Coast: a review. Mar. Geol. 245, 141–159. https://doi.org/10.1016/j.margeo.2007.06.001.

Castelle, B., Ruessink, B.G., Bonneton, P., Marieu, V., Bruneau, N., Price, T.D., 2010. Coupling mechanisms in double sandbar systems. Part 1: patterns and physical explanation. Earth Surf. Process. Landf. 35, 476–486. https://doi.org/10.1002/esp.1929.

Coco, G., Bryan, K.R., Geen, M.O., Ruessink, B.G., Turner, I.L., van Enckevort, I.M.J., 2005. Video observations of shoreline and sandbar coupled dynamics. Proc. Coasts Ports 471–476.

Dee, D.P., Uppala, S.M., Simmons, A.J., Berrisford, P., Poli, P., Kobayashi, S., Andrae, U., Balmaseda, M.A., Balsamo, G., Bauer, P., Bechtold, P., Beljaars, A.C.M., van de Berg, L., Bidlot, J., Bormann, N., Delsol, C., Dragani, R., Fuentes, M., Geer, A.J., Haimberger, L., Healy, S.B., Hersbach, H., Hólm, E.V., Isaksen, L., Kållberg, P., Köhler, M., Matricardi, M., McNally, A.P., Monge-Sanz, B.M., Morcrette, J.-J., Park, B.-K., Peubey, C., de Rosnay, P., Tavolato, C., Thépaut, J.-N., Vitart, F., 2011. The ERA-Interim reanalysis: configuration and performance of the data assimilation system. Q. J. R. Meteorol. Soc. 137, 553–597. https://doi.org/10.1002/qj.828.

van Enckevort, I.M.J., Ruessink, B.G., 2003. Video observations of nearshore bar behavior. Part 2: alongshore non-uniform variability. Cont. Shelf Res. 23, 513–532. https://doi.org/10.1016/S0278-4343(02)00235-2.

van Enckevort, I.M.J.J., Ruessink, B.G., Coco, G., Suzuki, K., Turner, I.L., Plant, N.G., Holman, R.A., 2004. Observations of nearshore crescentic sandbars. J. Geophys. Res. 109, C06028. https://doi.org/10.1029/2003JC002214.

García-Rubio, G., Huntley, D., Russell, P., 2015. Evaluating shoreline identification using optical satellite images. Mar. Geol. 359, 96–105. https://doi.org/10.1016/j.margeo.

2014.11.002.
Garrett, C., Toulany, B., 1981. Variability of the flow through the Strait of Belle Isle. J. Mar. Res. 39, 163–189.
Gorelick, N., Hancher, M., Dixon, M., Ilyushchenko, S., Thau, D., Moore, R., 2017. Google Earth Engine: planetary-scale geospatial analysis for everyone. Remote Sens. Environ. https://doi.org/10.1016/j.rse.2017.06.031.
Hagenaars, G., de Vries, S., Luijendijk, A.P., de Boer, W.P., Reniers, A.J.H.M., 2018. On the accuracy of automated shoreline detection derived from satellite imagery: a case study of the sand motor mega-scale nourishment. Coast. Eng. 133, 113–125. https://doi.org/10.1016/j.coastaleng.2017.12.011.
Holman, R.A., Symonds, G., Thornton, E.B., Ranasinghe, R., 2006. Rip spacing and persistence on an embayed beach. J. Geophys. Res. Oceans 111, 1–17. https://doi.org/10.1029/2005JC002965.
Homma, M., Sonu, C., 1962. Rhythmic pattern of longshore bars related to sediment characteristics. Coast. Eng. Proc. 248–278.
Kuriyama, Y., Ito, Y., Yanagishima, S., 2008. Medium-term variations of bar properties and their linkages with environmental factors at Hasaki, Japan. Mar. Geol. https://doi.org/10.1016/j.margeo.2007.10.006.
Lippmann, T.C., Holman, R.A., 1989. Quantification of sand bar morphology: a video technique based on wave dissipation. J. Geophys. Res. Oceans 94, 995–1011. https://doi.org/10.1029/JC094iC01p00995.
Lippmann, T.C., Holman, R.A., 1990. The spatial and temporal variability of sand bar morphology. J. Geophys. Res. 95, 11575. https://doi.org/10.1029/JC095iC07p11575.
Markham, B.L., Jenstrom, D., Masek, J.G., Dabney, P., Pedelty, J.A., Barsi, J.A., Montanaro, M., 2016. Landsat 9: status and plans. In: Butler, J.J., Xiong, X., Gu, X. (Eds.), Earth Observing Systems XXI, pp. 99720G. https://doi.org/10.1117/12.2238658.
Orzech, M.D., Thornton, E.B., MacMahan, J.H., O'Reilly, W.C., Stanton, T.P., 2010. Alongshore rip channel migration and sediment transport. Mar. Geol. 271, 278–291. https://doi.org/10.1016/j.margeo.2010.02.022.
Orzech, M.D., Reniers, A.J.H.M., Thornton, E.B., MacMahan, J.H., 2011. Megacusps on rip channel bathymetry: observations and modeling. Coast. Eng. 58, 890–907. https://doi.org/10.1016/j.coastaleng.2011.05.001.
van Os, J., Caires, S., 2011. How to carry out metocean studies. In: Proceedings of the ASME 2011 30th International Conference on Ocean, Offshore and Arctic Engineering, pp. 47–57. https://doi.org/10.1115/OMAE2011-49066.
Pape, L., Plant, N.G., Ruessink, B.G., 2010. On cross-shore migration and equilibrium states of nearshore sandbars. J. Geophys. Res. Earth Surf. 115, 1–16. https://doi.org/10.1029/2009JF001501.
Pardo-Pascual, J.E., Almonacid-Caballer, J., Ruiz, L.A., Palomar-Vázquez, J., Palomar-Vazquez, J., 2012. Automatic extraction of shorelines from Landsat TM and ETM+ multi-temporal images with subpixel precision. Remote Sens. Environ. 123, 1–11. https://doi.org/10.1016/j.rse.2012.02.024.
Plant, N.G., Holman, R.A., Freilich, M.H., Birkemeier, W.A., 1999. A simple model for interannual sandbar behavior. J. Geophys. Res. Oceans 104, 15755–15776. https://doi.org/10.1029/1999JC900112.
Plant, N.G., Holland, K.T., Holman, R.A., 2006. A dynamical attractor governs beach response to storms. Geophys. Res. Lett. 33, 1–6. https://doi.org/10.1029/2006GL027105.
Price, T.D., Ruessink, B.G., 2013. Observations and conceptual modelling of morphological coupling in a double sandbar system. Earth Surf. Process. Landf. 38, 477–489. https://doi.org/10.1002/esp.3293.
Price, T.D., Ruessink, B.G., Castelle, B., 2014. Morphological coupling in multiple sandbar systems — a review. Earth Surf. Dyn. 2, 309–321. https://doi.org/10.5194/esurf-2-309-2014.
Ranasinghe, R., Symonds, G., Black, K., Holman, R., 2004. Morphodynamics of intermediate beaches: a video imaging and numerical modelling study. Coast. Eng. 51, 629–655. https://doi.org/10.1016/j.coastaleng.2004.07.018.
Ribas, F., Garnier, R., Ojeda, E., Falqués, A., Guillén, J., Calvete, D., 2007. Observation and modeling of crescentic bars in Barcelona embayed beaches. Coast. Sediments 7, 2111–2123.
Ruessink, B.G., Van Enckevort, I.M.J., Kingston, K.S., Davidson, M.A., 2000. Analysis of observed two- and three-dimensional nearshore bar behaviour. Mar. Geol. 169, 161–183. https://doi.org/10.1016/S0025-3227(00)00060-8.
Ruessink, B.G., Coco, G., Ranasinghe, R., Turner, I.L., 2007a. Coupled and noncoupled behavior of three-dimensional morphological patterns in a double sandbar system. J. Geophys. Res. Oceans 112, 1–11. https://doi.org/10.1029/2006JC003799.
Ruessink, B.G., Kuriyama, Y., Reniers, A.J.H.M.H.M., Roelvink, J.A., Walstra, D.J.R., 2007b. Modeling cross-shore sandbar behavior on the timescale of weeks. J. Geophys. Res. Earth Surf. 112. https://doi.org/10.1029/2006JF000730.
Rutten, J., Ruessink, B.G., Price, T.D., 2018. Observations on sandbar behaviour along a man-made curved coast. Earth Surf. Process. Landf. 43, 134–149. https://doi.org/10.1002/esp.4158.
de Schipper, M.A., Ranasinghe, R., Reniers, A., Stive, M., 2011. On the initiation of nearshore morphological rhythmicity. In: Coastal Engineering Proceedings. 47https://doi.org/10.9753/icce.v32.sediment.47. sediment.
Shen, X., Liu, B., Li, Q.-Q., 2017. Correcting bias in the rational polynomial coefficients of satellite imagery using thin-plate smoothing splines. ISPRS J. Photogramm. Remote Sens. 125, 125–131. https://doi.org/10.1016/j.isprsjprs.2017.01.007.
Short, A.D., 1985. Rip-current type, spacing and persistence, Narrabeen Beach, Australia. Mar. Geol. https://doi.org/10.1016/0025-3227(85)90046-5.
Smit, M., Reniers, A.J.H.M., Stive, M.J.F., 2011. What determines nearshore sandbar response? In: Coastal Engineering Proceedings. 56https://doi.org/10.9753/icce.v32.sediment.56. sediment.
Sonu, C.J., 1973. Three-dimensional beach changes. J. Geol. 81, 42–64.
Splinter, K.D., Holman, R.A., Plant, N.G., 2011. A behavior-oriented dynamic model for sandbar migration and 2DH evolution. J. Geophys. Res. Oceans 116, 1–21. https://doi.org/10.1029/2010JC006382.
Van de Lageweg, W.I., Bryan, K.R., Coco, G., Ruessink, B.G., 2013. Observations of shoreline-sandbar coupling on an embayed beach. Mar. Geol. 344, 101–114. https://doi.org/10.1016/j.margeo.2013.07.018.
Walstra, D.J.R., Reniers, A.J.H.M., Ranasinghe, R., Roelvink, J.A., Ruessink, B.G., 2012. On bar growth and decay during interannual net offshore migration. Coast. Eng. https://doi.org/10.1016/j.coastaleng.2011.10.002.
Walstra, D.-J., Wesselman, D., van der Deijl, E., Ruessink, G., 2016. On the intersite variability in inter-annual nearshore sandbar cycles. J. Mar. Sci. Eng. 4, 15. https://doi.org/10.3390/jmse4010015.
Wright, L.D., Short, A.D., 1984. Morphodynamic variability of surf zones and beaches: a synthesis. Mar. Geol. 56, 93–118. https://doi.org/10.1016/0025-3227(84)90008-2.